Development of Highly Effective CaO-based, MgO-stabilized CO_2 Sorbents via a Scalable "One-Pot" Recrystallization Technique

*Marcin Broda, Agnieszka M. Kierzkowska, and Christoph R. Müller**

Here, we report the development of novel, highly effective CaO-based CO_2 sorbents via a well-scalable and economic synthesis technique, viz. the re-crystallization of calcium and magnesium acetates in organic solvents. We successfully synthesized a material that possessed an excellent cyclic CO_2 uptake (10.71 mmol(CO_2) g(sorbent)$^{-1}$ after 10 cycles), even under harsh, but practically relevant, regeneration conditions. To obtain such a high cyclic CO_2 uptake, it was found to be crucial to mix the active component, CaO, and the high Tammann temperature support, MgO, on the nanometer scale. The synthesis technique developed only requires 8 wt% of MgO to effectively stabilize the cyclic CO_2 uptake of the material. Furthermore, we established the influence of various synthesis parameters such as the molar ratio of Ca^{2+} to Mg^{2+} and the re-crystallization media on the sorbent's morphology and, in turn, cyclic CO_2 uptake. Our best material exceeded the CO_2 uptake (10th cycle) of limestone by 200%.

1. Introduction

The World Energy Outlook of 2012[1] predicts that the global CO_2 emissions from fuel combustion will increase by 22% over the next 25 years, reaching 37 Gt CO_2 in 2035. A strategy to reduce carbon dioxide emissions from fossil fuel fired power stations is the implementation of CO_2 capture and storage (CCS).[2–4] However, the currently technologically available CCS process, i.e., scrubbing with amines is potentially prohibitively expensive.[5] Therefore, substantial research activities are currently undertaken to develop less costly CO_2 capture processes[6–8], e.g., utilizing the cyclic carbonation and calcination reactions of CaO and $CaCO_3$, respectively[4]:

$$CaO + CO_2 \leftrightarrow CaCO_3, \Delta H^{\circ}_{298K} = \pm 178 \text{ kJ / mol} \quad (1)$$

CaO is a very attractive CO_2 sorbent owing to (i) the low costs of naturally occurring CaO precursors, e.g., limestone, (ii) its high theoretical CO_2 absorption capacity of 17.8 mmol(CO_2) g(sorbent)$^{-1}$ and (iii) its sufficient mechanical strength, thus, allowing it to be used in fluidized bed reactors.[4] However, limestone derived CaO comes with a major disadvantage, i.e., its rapid decrease in CO_2 uptake capacity with cycle number due to thermal sintering. The Tammann temperature of $CaCO_3$ is only 533 °C[9], which is comparatively low when compared to the expected operating temperatures (650–950 °C). Thermal sintering results in a dramatic reduction in the available surface area and volume in pores with diameters <100 nm.[10] The importance of the available pore volume becomes apparent if the two regimes of the carbonation reaction are considered.[10] A first, fast and kinetically limited reaction stage associated with the filling of pores of diameter d_{pore} <100 nm by newly formed $CaCO_3$ is followed by a substantially slower reaction stage in which the reaction rate is controlled by the (slow) diffusion of CO_2 through the $CaCO_3$ product layer. The transition between the two reaction regimes occurs at a critical product layer thickness of ~50 nm.[11] However, the formation of a homogeneously growing product layer of $CaCO_3$ on the surface of CaO is possibly an over-simplification. In a recent study, Li et al.[12] applied rate equation theory to describe the nucleation and growth of $CaCO_3$ product islands on the surface of CaO during carbonation. It was found that in the initial reaction stage CaO reacts quickly with CO_2 and the newly formed $CaCO_3$ islands gradually cover the CaO surface. Here, the growth of the product islands involves the diffusion of $CaCO_3$ molecules or ions (CO_3^{2-})[13] along the CaO surface and the boundary between the solid reactant and product. Once the CaO surface is fully covered with the $CaCO_3$ product, the reaction enters a substantially slower reaction stage, which is controlled by the diffusion of CO_2 through the $CaCO_3$ product layer. The transition between the fast and the slow reaction regime occurs at a critical CaO conversion. This transition could be interpreted simplistically as a critical product layer thickness as proposed by Alvarez and Abanades[11]. Li et al.[12] reported that the critical CaO conversion increases with reaction temperature. This observation was explained by the fact that an increase in reaction temperature enhances surface diffusion and results in the formation of larger $CaCO_3$ islands (whereas the island density decreases), thus, increasing the surface area of CaO available for reaction with CO_2. Taking into account the typically short contacting times in fluidized bed reactors, only the CO_2 uptake achieved during the fast reaction regime

M. Broda, Dr. A. M. Kierzkowska, Prof. C. R. Müller
Laboratory of Energy Science and Engineering
ETH Zurich
Leonhardstrasse 27, 8092, Zurich, Switzerland
E-mail: muelchri@ethz.ch

DOI: 10.1002/adfm.201400862

will be of practical relevance. In recent years different strategies to overcome the dramatic loss in the cyclic CO_2 uptake of CaO derived from naturally occurring precursors have been assessed, e.g., thermal pretreatment[14] or hydration[15]. However, Manovic et al.[16] noticed that reactivation via hydration substantially reduces the mechanical stability of the sorbent resulting in high rates of attrition. An alternative approach is the development of synthetic CaO-based CO_2 sorbents which minimize thermal sintering.[17–23] To ensure a high and thermally stable surface area and pore volume, CaO is typically supported on a high Tammann temperature material, e.g., MgO, Al_2O_3, or ZrO_2. For example, Li et al.[17] prepared a CO_2 sorbent by mixing CaO and $Al(NO_3)_3$ into a solution of distilled water and 2-propanol. Upon drying and calcination, the best material (CaO : $Ca_{12}Al_{14}O_{33}$ = 75:25 wt%) possessed a CO_2 uptake of 10.20 mmol(CO_2) g(sorbent)$^{-1}$ after 13 cycles. In a further study Lu et al.[18] stabilized CaO on various supports, viz. SiO_2, CoO, ZrO_2, Cr_2O_3, TiO_2, and CeO_2, using flame spray pyrolysis. ZrO_2 was identified as the most promising support and a CaO conversion of 0.44 mol(CO_2) mol(CaO)$^{-1}$ after 100 cycles (Ca^{2+}:Zr^{4+} = 5:1) was reported. The favourable CO_2 capture characteristics of the material were attributed to the formation of a well-dispersed, high Tammann temperature matrix ($CaZrO_3$) that ensured the stability of nano-sized CaO particles over multiple reaction cycles.[18] Recently, Broda et al.[19] employed a sol-gel technique to develop Al_2O_3-supported, CaO-based sorbents. After 30 cycles the best sorbent synthesized (Ca^{2+}:Al^{3+} = 90:10) possessed a CO_2 uptake of 11.55 mmol(CO_2) g(sorbent)$^{-1}$, a value that is ~ 150% higher than that of limestone. Broda et al.[19] also studied in detail the influence of the ratio Ca^{2+} : Al^{3+} on the morphology and the CO_2 capture characteristics of the materials. It was found that decreasing the ratio of Ca^{2+} to Al^{3+} gave CO_2 sorbents with a higher surface area and pore volume, but also an overall reduced CO_2 uptake due to the lower quantity of CO_2 capture active CaO.

With regards to synthetic CaO-based CO_2 sorbents, the majority of work reported has largely applied synthesis techniques that do not allow mixing CaO and the support material on a nanometre level. Furthermore, the synthesis techniques employed are often only poorly scalable since they frequently involve several reaction steps or even multiple reactors and the synthetic sorbents developed have often only marginally exceeded the CO_2 capture capacity of limestone. In this work we have developed a novel and well-scalable technique, viz. the re-crystallization of calcium and magnesium acetates, to synthesize highly effective CaO-based CO_2 sorbents. The "one-pot" synthesis technique reported here, allows the stabilization of CaO on an inert, high Tammann temperature MgO matrix. The influence of various synthesis parameters such as the molar ratio of Ca^{2+} to Mg^{2+} and the re-crystallization media on the sorbent's morphology and, in turn, CO_2 capture characteristics are critically assessed.

2. Results and Discussion

First, the influence of different synthesis parameters, i.e., the calcium precursor used, the molar ratio of Ca^{2+} to Mg^{2+} and the re-crystallization media, on the morphology of the CaO-based sorbents was assessed using N_2 adsorption measurements. From **Table 1** it can be seen that calcium acetate re-crystallized in pentanol possessed a BET surface area of 39 m^2 g^{-1} and a BJH pore volume of 0.17 cm^3 g^{-1}. On the other hand, a comparatively low surface area and pore volume of 6 m^2 g^{-1} and 0.02 cm^3 g^{-1}, respectively, was obtained for Ca_methanol_100:0. Also materials re-crystallized from alkanes and toluene possessed a relatively low surface area and pore volume. N_2 adsorption measurements also confirm that decreasing the molar ratio of Ca^{2+} to Mg^{2+} increased the surface area and pore volume of the material. For example, Ca_pentanol_90:10 and Ca_pentanol_50:50 possessed a surface area of, respectively, 29 m^2 g^{-1} and 49 m^2 g^{-1}, and a pore volume of 0.06 cm^3 g^{-1} and 0.12 cm^3 g^{-1}. This observation is in line with the high surface area of magnesium acetate recrystallized in pentanol, i.e., the surface area of Mg_pentanol_100:0 was 323 m^2 g^{-1}. On the contrary, the surface area of commercial calcium acetate (Acros Organics) was 3 m^2 g^{-1}.

Table 1. BET surface area and BJH pore volume of the different CO_2 sorbents studied.

Material	BET surface area [m^2/g]	BJH pore volume [cm^3/g]
Ca_pentanol_100:0	39	0.17
Ca_ethanol_100:0	25	0.06
Ca_metanol_100:0	6	0.02
Ca_hexane_100:0	5	0.02
Ca_toluene_100:0	3	0.05
Ca_pentanol_90:10	29	0.06
Ca_pentanol_50:50	49	0.12
Mg_pentanol_100:0	323	0.02
Commercial calcium acetate	3	0.02
Ca_90:10	3	0.02
Calcined limestone	21	0.28

Next, scanning electron microscopy (SEM) images of commercial and recrystallized calcium acetate using different solvents are shown in **Figures 1** and S1. As reference also a micrograph of limestone is given in Figure 1. Commercial calcium acetate has a characteristic heterogeneous and comparatively coarse structure (Figure 1(a)). In contrast, calcium acetate is recrystallized in methanol in the form of hexagonal crystals (11.1 ± 8.5 µm average edge length and 3 ± 1.4 µm thickness), Figure 1(b). The re-crystallization of calcium acetate in pentanol or ethanol, Figures 1(c) and S1(a), respectively, yields rod-shaped crystals. Based on the analysis of 30 rods, the average length of a rod was determined as 52.6 ± 19.4 µm and 40.0 ± 26.3 µm (diameter of 690 ± 44 nm and 595 ± 37 nm) for Ca_ethanol_100:0 and Ca_pentanol_100:0, respectively. For the case that calcium acetate was recrystallized in alkanes (Figures 1(d) and S1(b)) or toluene (Figure S1(c)) coarse and rather heterogeneous structures were obtained. The formation of well-defined, rod-shaped crystals of calcium acetate leads to a material with a high surface area compared to Ca_hexane_100:0 and Ca_toluene_100:0 that are characterized by a fairly coarse and

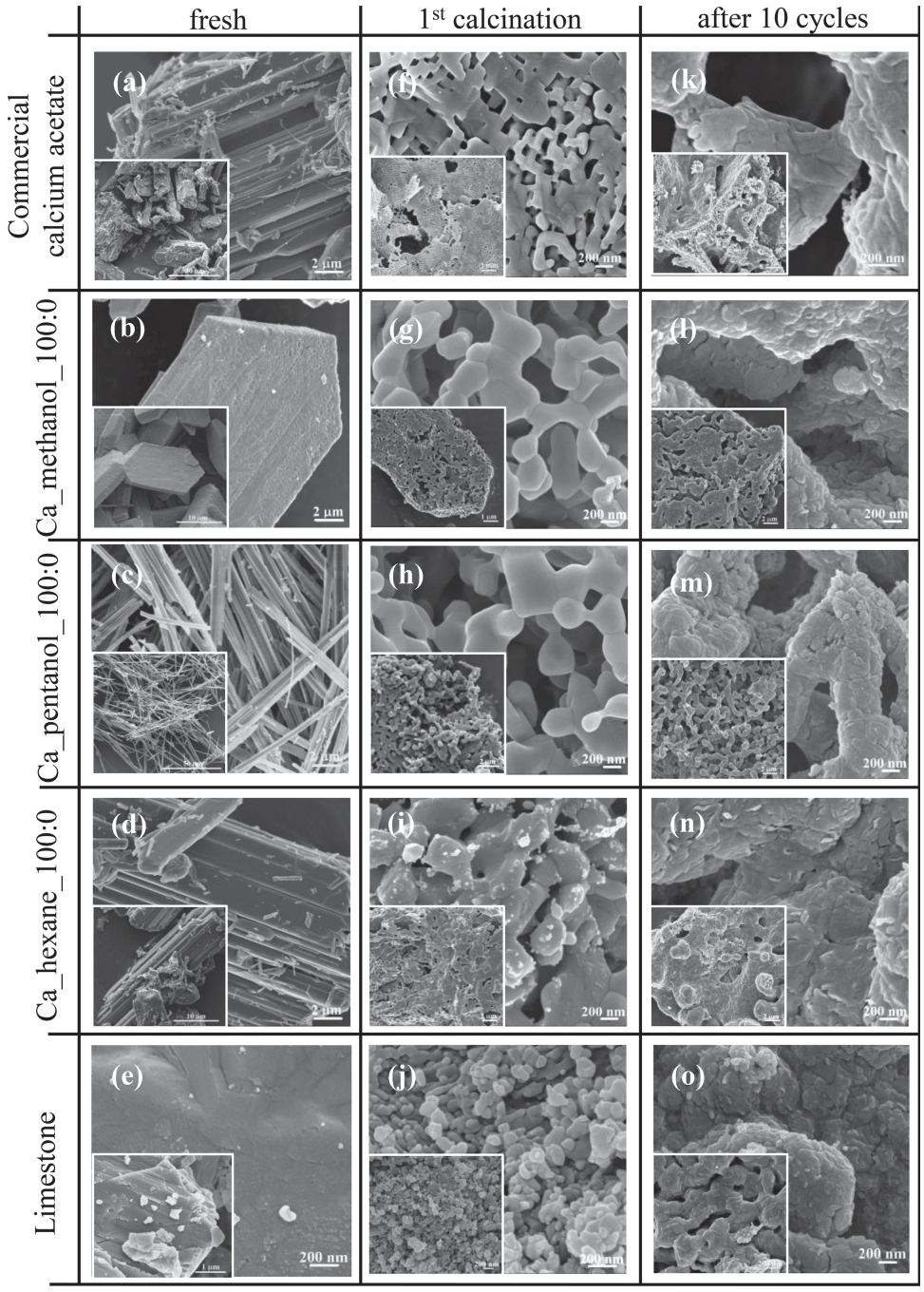

Figure 1. SEM images of pure, i.e., unsupported, calcium acetate: fresh, calcined and after being exposed to 10 carbonation-calcination cycles. The micrographs of calcined and reacted limestone were plotted for comparison.

poorly defined morphology (Table 1). One would expect that the polarity of the solvents, characterised by the normalized solvent parameter (E_T^N), influences the re-crystallization characteristics of calcium acetate. Alcohols such as 1-pentanol E_T^N = 0.568) or ethanol (E_T^N = 0.654) show polar properties, whereas alkanes (e.g., hexane with E_T^N = 0.009) and toluene E_T^N = 0.099) are apolar.[24,25] Highly polar alcohols partially dissolve calcium acetate,[26] whereas apolar solvents such as hexane or toluene inhibit the dissolution of calcium acetate (Figure 1(d) and S1(c)). Figure 1 shows clearly that the type of alcohol used, possibly through differences in their boiling point and polar properties (methanol has the highest polarity among the alcohols tested here),[24] influences the morphology of the re-crystallized calcium acetate. This hypothesis is supported by the work of van der Sluis et al.[27] who investigated the crystallization of calcium acetate from pure water or ethanol-water solutions. The authors reported that crystallization from pure water yielded needle-shaped crystals of calcium acetate monohydrate.[27] The

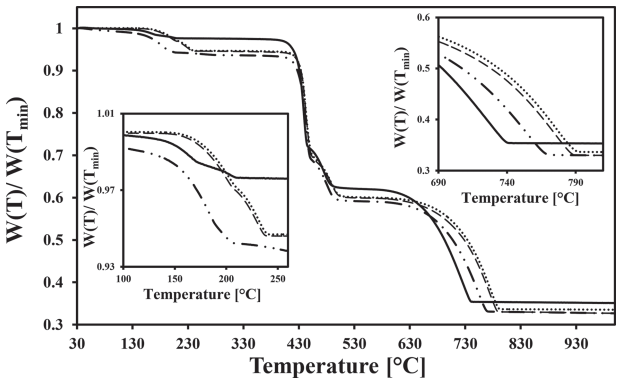

Figure 2. Normalized weight change as a function of temperature during N_2-TPD: (-··-) Ca_methanol_100:0, (—) Ca_pentanol_100:0, (- -) Ca_hexane_100:0 and (···) commercial calcium acetate hydrate. The temperature ramp was 10 °C $(min)^{-1}$ with T_{min} = 30 °C and T_{max} = 1000 °C.

addition of 10% ethanol to water decreased the solubility of calcium acetate and resulted in the crystallization of large flat needles.[27] Methanol has also the lowest boiling point (65 °C) among all the alcohols studied here. It is believed that this temperature is too low to effectively dehydrate the calcium precursor during recrystallization. This is confirmed by **Figure 2**, which plots the normalized weight change of re-crystallized calcium acetate as a function of temperature during N_2-TPD. The influence of the degree of calcium acetate hydration on its morphology has been studied by Saury et al.[28]. It was found that calcium acetate hemihydrate possessed coarse and poorly defined structures, whereas well-defined elongated rods were observed for calcium acetate monohydrate.[28]

As shown in Figure 2, all calcium acetates revealed three distinctive decomposition steps: Ca_methanol_100:0, Ca_penthanol_100:0, Ca_hexane_100:0, and commercial calcium acetate dehydrate to anhydrous calcium acetate in the temperature ranges of 100–210 °C, 120–210 °C, 140–240 °C, and 140–245 °C, respectively. For Ca_hexane_100:0 and Ca_methanol_100:0 the mass loss due to dehydration was, respectively, ~5.5 and ~5.6 wt%, which compares very well to the theoretically expected value of 5.4 wt%, i.e., one water molecule for every two calcium acetate molecules. In contrast, the loss of one water molecule for every four calcium acetate molecules, i.e., ~2.7 wt%, was determined for Ca_pentanol_100:0. Subsequently, anhydrous calcium acetate decomposes into $CaCO_3$ in the temperature range of 390–510 °C, independent of synthesis conditions. The decomposition of $CaCO_3$ into CaO occurred in the temperature range of 580–770, 570–740, 600–785, and 620–790 °C for, respectively, Ca_methanol_100:0, Ca_penthanol_100:0, Ca_hexane_100:0, and commercial calcium acetate.

The micrographs of the fresh (Figures 1(a-d)) and calcined materials (Figures 1(f–i)) show severe morphological changes after calcination at 750 °C. For example, after the calcination of Ca_pentanol_100:0 and Ca_hexane_100:0 at 750 °C, Figures 1(h,i), the resulting CaO was comprised of an assembly of grains with an average diameter of 289 ± 36 nm and 380 ± 130 nm, respectively. After 10 repeated cycles of the carbonation and calcination reaction, Figures 1(k–n), the grains grew in size with the structure of cycled Ca_hexane_100:0 being fairly non-porous. However, also the morphologies of the reference material, i.e., fresh, unreacted and reacted limestone differed substantially (Figures 1(e,j,o)). After calcination, limestone was comprised of grains with an average size of 103 ± 5 nm. Cycled limestone completely lost its nano-structured morphology, in agreement with previous reports.[29]

Lastly, the different unsupported sorbents were assessed with regards to their cyclic CO_2 capture characteristics, defined as mmol(CO_2 captured) (g of calcined sorbent)$^{-1}$. For comparison, the performance of limestone and commercial calcium acetate is also included in **Figure 3**. Limestone possessed a high CO_2 uptake of 14.21 mmol(CO_2) g(sorbent)$^{-1}$ in the 1st cycle which, however, rapidly decreased to 7.14 mmol(CO_2)

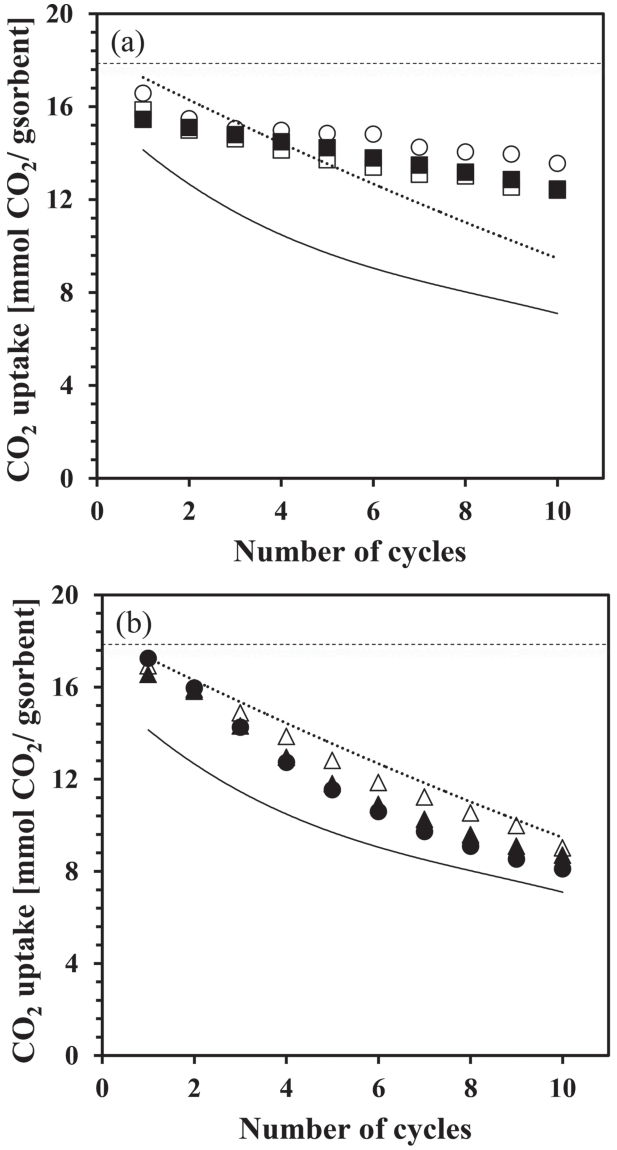

Figure 3. CO_2 uptake characteristics of unsupported CaO-based sorbents re-crystalized in (a) alcohols and (b) alkanes or toluene determined in a TGA: (■) Ca_methanol_100:0, (□) Ca_ethanol_100:0, (○) Ca_pentanol_100:0, (●) Ca_pentane_100:0, (Δ) Ca_hexane_100:0, (▲) Ca_toluene_100:0, (···) commercial calcium acetate and (—) limestone. The carbonation and calcination reactions were performed isothermally at 750 °C. The dashed line (- - -) gives the theoretical CO_2 uptake of pure CaO.

g(sorbent)$^{-1}$ after 10 cycles. The rapid decrease in the CO_2 uptake of limestone is well established and has been reported previously.[4] Commercial calcium acetate showed a significantly higher CO_2 uptake than limestone in the 1st cycle, viz. 17.07 mmol(CO_2) g(sorbent)$^{-1}$: a value that is very close to the theoretical maximum of 17.8 mmol(CO_2) g(sorbent)$^{-1}$. However, with cycle number the CO_2 uptake decreased to only 9.66 mmol(CO_2) g(sorbent)$^{-1}$ after 10 cycles. Turning now to the recrystallized CO_2 sorbents, the highest CO_2 uptake in the 1st and 10th cycle of, respectively, 16.58 and 13.56 mmol(CO_2) g(sorbent)$^{-1}$, was measured for calcium acetate re-crystallized from 1-pentanol. For Ca_pentanol_100:0 the average decay rate of the CO_2 uptake with cycle number was only 1.9% per cycle (as determined from the 10 cycles experiment), a value that is roughly 230% lower than that of commercial calcium acetate.

The cyclic CO_2 uptake of the materials re-crystallized in alkanes or toluene is plotted in Figure 3(b). The highest initial CO_2 uptake of 17.24 mmol(CO_2) g(sorbent)$^{-1}$ was determined for Ca_pentane_100:0. However, with cycle number its CO_2 uptake drastically decreased yielding only 8.11 mmol(CO_2) g(sorbent)$^{-1}$ after 10 cycles. For the materials recrystallized in alkanes, the highest CO_2 uptake (9.02 mmol(CO_2) g(sorbent)$^{-1}$ after 10 cycles) was measured for Ca_hexane_100:0, exceeding the CO_2 capture capacity of limestone by approximately 30%. The decrease in the cyclic CO_2 uptake of the recrystallized, but unsupported materials is in agreement with the severe morphological changes occurring on repeated calcination and carbonation steps as revealed by SEM (Figures 1(k–n)).

The substantially higher cyclic CO_2 uptake of calcium acetates recrystallized from alcohols when compared to calcium acetates recrystallized from alkanes or toluene can be attributed to their higher porosity and, thus, lower susceptibility to sintering. This is in line with a report of Borgwardt[30] who investigated the rate of sintering of CaO derived from both $Ca(OH)_2$ and limestone and observed a significantly higher sintering rate for CaO prepared from $Ca(OH)_2$ than for limestone-derived CaO. Borgwardt[30] explained this observation by the lower porosity of CaO derived from $Ca(OH)_2$, resulting in a closer contact between the individual CaO grains and, thus, creating a greater propensity for neck formation.

To increase the thermal stability of the morphology of the recrystallized materials and, in turn, their cyclic CO_2 capture capacity, attempts were made to support CaO on an inert, high Tammann temperature material (MgO) on the nanometer scale. As shown in **Figure 4**, the addition of Mg^{2+} strongly affected the morphology of the materials re-crystallized in 1-pentanol. The material that contained a molar ratio of Ca^{2+}:Mg^{2+} = 90:10, Figure 4(a), possessed a rod-like morphology, similar to pure calcium acetate, Figure 1(c). Decreasing the ratio of Ca^{2+} to Mg^{2+} to 70:30 and 50:50, Figures 4(b,c), resulted in the formation of separate crystals (320 ± 87 and 301 ± 59 nm, respectively) of magnesium acetate that cover the surface of coarse, micrometre-sized calcium acetate, as confirmed by energy-dispersive X-ray (EDX) imaging (**Figure 5**). For comparison, a SEM image of mechanically mixed calcium and magnesium acetate with a molar ratio of Ca^{2+}:Mg^{2+} = 90:10 (denoted as Ca_90:10) is given in Figure 4(d). Fresh Ca_90:10 is composed of a mixture of comparatively coarse, i.e., micrometer-sized crystals of $Ca(C_2H_3O_2)_2$ and $Mg(C_2H_3O_2)_2$. However, similar to pure calcium acetate, calcination at 750 °C led to substantial morphological changes. After calcination an assembly of grains with an average size of 153 ± 59, 89 ± 30 and 108 ± 35 nm for, respectively, Ca_pentanol_90:10, Ca_pentanol_70:30 and Ca_pentanol_50:50, was obtained. Significantly larger grains (average size of 241 ± 73 nm), partially of molten appearance, were observed for Ca:Al_90:10. The chemical composition and crystallinity of the MgO-supported CO_2 sorbents was probed at different stages of the carbonation-calcination cycles (**Figure 6**). As expected, the calcined CO_2 sorbent (Ca^{2+}:Mg^{2+} = 50:50, re-crystallized in pentanol) contained lime (CaO) and periclase (MgO). The crystallite size of CaO and MgO in Ca_pentanol_50:50 was determined as 38 nm and 24 nm, respectively. Using XRD the presence of a mixed oxide of CaO and MgO could not be observed. This observation is in agreement with observations of Britton et al.[31] showing that the calcination of dolomite in the temperature range 640–720 °C leads to an intermediate solid solution (Mg,Ca)O that, however, quickly segregates into different crystals of CaO and MgO. The diffractogram of the carbonated material, Figure 6(b), shows the presence of calcite ($CaCO_3$), periclase (MgO) and portlandite ($Ca(OH)_2$). Thermodynamic calculations confirm that under the carbonation conditions studied here, $MgCO_3$ does not form. Thus, periclase is inert with respect to the carbonation reaction, i.e., it does not participate in the capture and release of CO_2. The presence of small amounts of portlandite in the diffractograms of the calcined material is due to the very hygroscopic nature of CaO. Figures 4(i–l) show CaO-based, MgO-stabilized CO_2 sorbents which have undergone 10 repeated carbonation-calcination cycles. For Ca_pentanol_70:30 and Ca_pentanol_50:50 the morphology did not change appreciably when compared to the morphologies observed after the first calcination step. On the other hand, over repeated carbonation-calcination cycles Ca_pentanol_90:10 developed a morphology characterised by fine grains. Based on the analysis of 30 grains, the average grain sizes of Ca_pentanol_90:10, Ca_pentanol_70:30 and Ca_pentanol_50:50 were determined as, respectively, 105 ± 44, 110 ± 36 and 108 ± 32 nm. In contrast, cycled Ca_90:10 lost its initial morphology due to severe sintering, accompanied by a growth of the voids incorporated in the grain structure, Figure 4(l).

The stabilizing effect of MgO (Tammann temperature (T_T) = 1290 °C[32] on the CO_2 uptake characteristics of CaO is demonstrated in Figures S2 and 7. Figure S2 shows that Ca_90:10 possessed the highest CO_2 uptake of 15.62 mmol(CO_2) g(sorbent)$^{-1}$ in the first cycle. However, with increasing cycle number the CO_2 uptake decreased rapidly and after 10 cycles the CO_2 uptake was reduced to 9.99 mmol(CO_2) g(sorbent)$^{-1}$. Thus, the average decay rate of the CO_2 uptake with cycle number was 3.6% per cycle as determined from the 10 cycles experiment. After 10 cycles the highest CO_2 uptake of 12.75 mmol(CO_2) g(sorbent)$^{-1}$ was determined for Ca_pentanol_90:10. Decreasing the molar ratio of Ca^{2+} to Mg^{2+} resulted in a decrease in the overall CO_2 uptake, albeit accompanied by an improved stability of the material, e.g., in the 1st and 10th cycle the CO_2 uptake of Ca_pentanol_70:30 was 12.39 and 11.90 mmol(CO_2) g(sorbent)$^{-1}$, respectively.

To determine the stability of the CO_2 sorbents under practically relevant calcination temperatures, 10 carbonation-calcination cycles were conducted in a TGA using a calcination

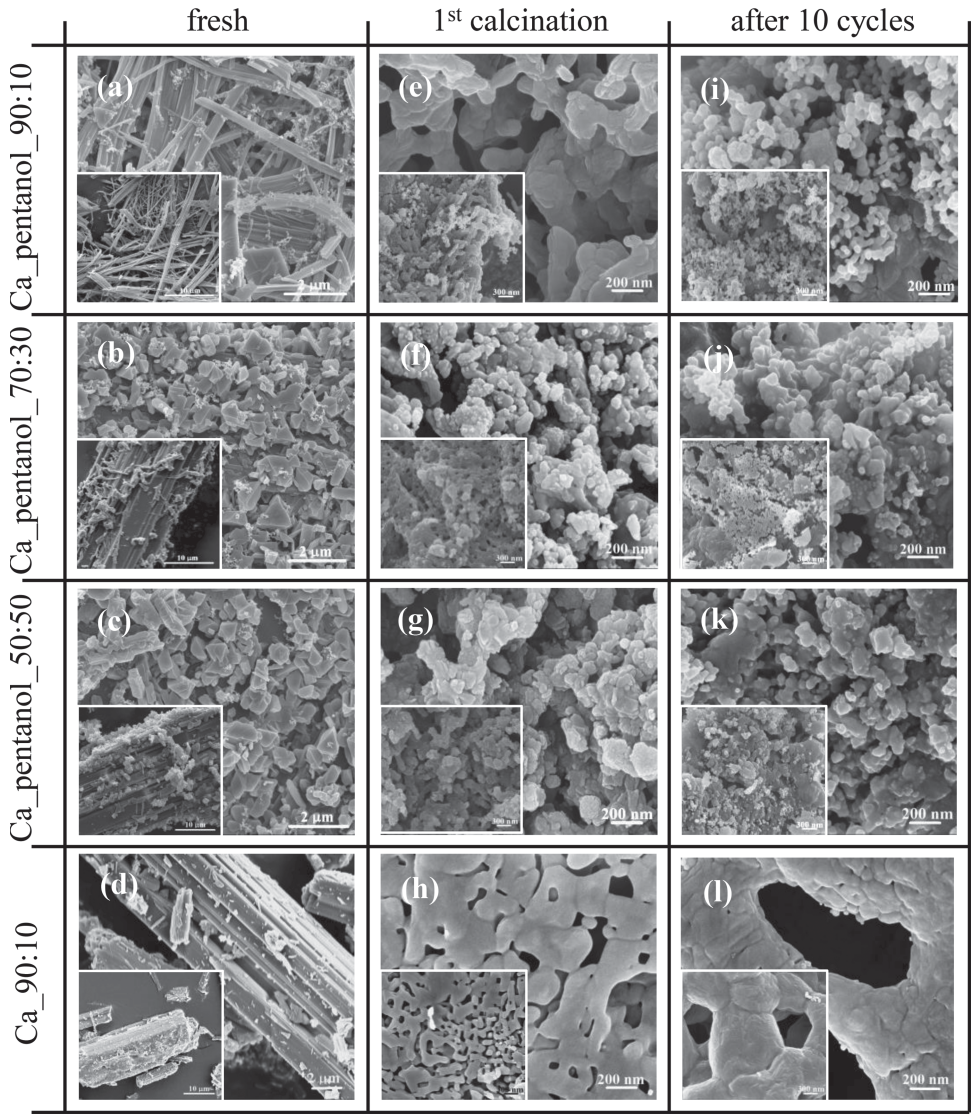

Figure 4. SEM images of Mg-supported calcium acetate: fresh, calcined and after being exposed to 10 carbonation-calcination cycles.

temperature of 900 °C. In these experiments the calcination reaction was performed in a pure CO_2 atmosphere, i.e., the partial pressure of CO_2 was 1 bar. **Figure 7** reveals that under these calcination conditions the CO_2 uptake of Ca_90:10 decreased even more rapidly yielding only 5.45 mmol(CO_2) g(sorbent)$^{-1}$ after 10 cycles. Lower CO_2 uptakes were also determined for the unsupported sorbents. For example, Ca_pentanol_100:0 and limestone possessed a CO_2 uptake of, respectively, 3.12 and 3.56 mmol(CO_2) g(sorbent)$^{-1}$ after 10 cycles. Stabilization of CaO with MgO using the re-crystallization technique reported here, resulted in markedly improved CO_2 uptakes. For example, the CO_2 uptake of Ca_pentanol_50:50 was 10.78 and 7.51 mmol(CO_2) g(sorbent)$^{-1}$ in the 1st and 10th cycle, respectively. After 10 cycles the highest CO_2 uptake of 10.71 mmol(CO_2) g(sorbent)$^{-1}$ was determined for Ca_pentanol_90:10, thus, exceeding the CO_2 uptake of the reference limestone by 200%.

We believe that the following two features of the new materials explain their favorable CO_2 capture characteristics. As described initially, the carbonation reaction is comprised of two regimes: a kinetically limited reaction stage associated with the filling of pores of diameter d_{pore} < 100 nm by newly formed $CaCO_3$, followed by a substantially slower reaction stage in which the reaction rate is controlled by the diffusion of CO_2 through the $CaCO_3$ product layer.[10] The transition between the fast and the slow reaction regime occurs at a critical CaO conversion that could be associated with a critical product layer thickness.[12] Thus, by nano-structuring a material, the extent of the diffusion-limited reaction stage of the carbonation reaction can be minimized. However, to maintain these favourable CO_2 capture characteristics beyond the first cycle, it is crucial to maintain the nano-structure of the material over repeated carbonation-calcination cycles. This is achieved via the incorporation of MgO on the nanometre scale. The SEM images presented in Figure 4 demonstrate convincingly that the re-crystallized materials studied here maintained their nanostructured morphology over 10 repeated

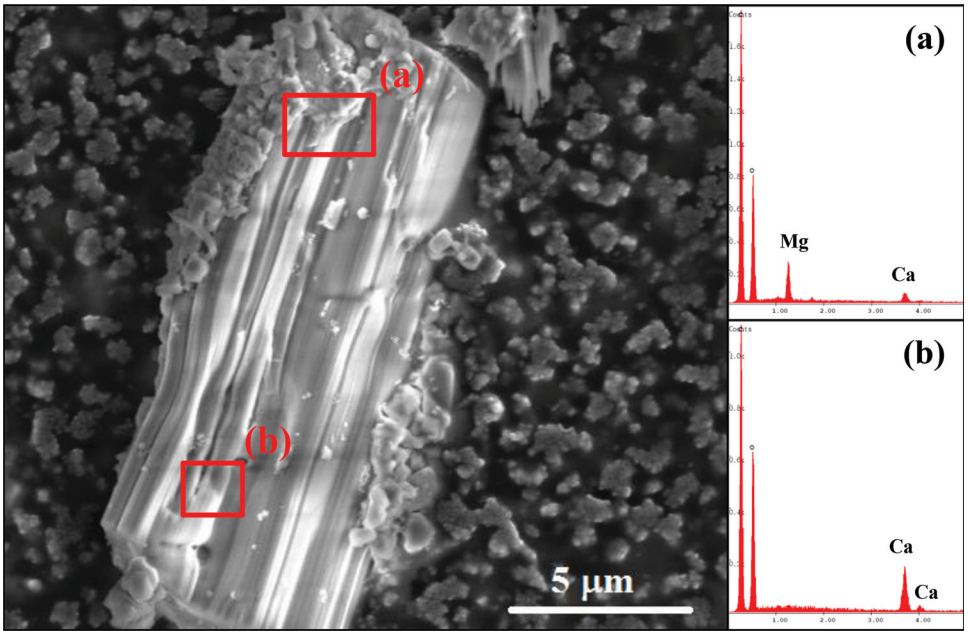

Figure 5. SEM image and EDX spectra obtained at different locations of Ca_pentanol_70:30.

cycles. Indeed, the morphology of Ca_pentanol_90:10 became even more "developed" with cycle number. On the other hand, the reference Ca_90:10 which was primarily comprised of separate crystals of $Ca(C_2H_3O_2)_2$ and $Mg(C_2H_3O_2)_2$, exhibited dramatic morphological changes, resulting in the formation of comparatively large, micrometre-sized grains (Figure 4(l)). This in turn led to a rapid decrease in the cyclic CO_2 uptake capacity of Ca_90:10. This observation is in agreement with the report of Filitz et al.[20] who found that sorbents in which Ca^{2+} and Mg^{2+} were mixed on a molecular level, i.e., similar to natural dolomite, showed a very high and stable CO_2 uptake. On the other hand, the formation of discrete crystals of $CaCO_3$ and $MgCO_3$ polymorphs led to a rapid decrease in the cyclic CO_2 uptake.

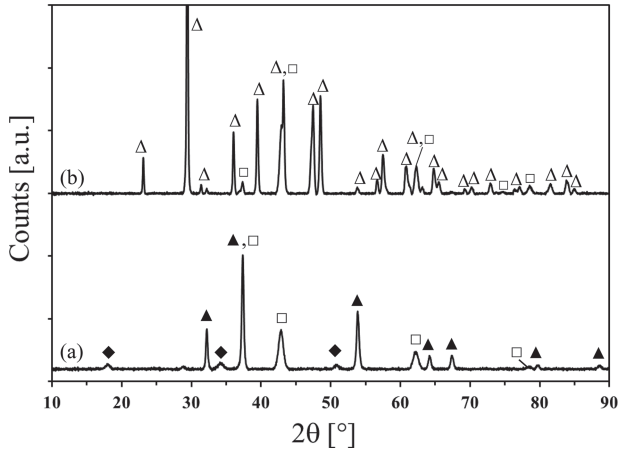

Figure 6. X-ray diffraction patterns: (a) calcined Ca_pentanol_50:50, (b) carbonated Ca_pentanol_50:50. The following compounds were identified: (▲) – lime, CaO, (Δ) – calcite, $CaCO_3$, (◆) – portlandite, $Ca(OH)_2$, (□) – periclase, MgO.

The influence of the calcination temperature on the CO_2 uptake is given in Figures 3, 7 and S2. Ridha et al.[33] demonstrated experimentally that both a high calcination temperature (≥900 °C) and a calcination atmosphere with a high CO_2 partial pressure, i.e., operating conditions that are representative of a practical CCS unit, promote thermal sintering and, hence, accelerate the decrease in the cyclic CO_2 capture capacity of the sorbent. For example, after 10 cycles Ca_pentanol_90:10 possessed a CO_2 uptake of 12.75 and 10.71 mmol(CO_2) g(sorbent)$^{-1}$ for calcination temperatures of 750 °C and 900 °C, respectively. However, the effect of the calcination temperature on the CO_2 uptake was significantly more pronounced for unsupported CaO, e.g., limestone. Here, increasing the calcination temperature from 750 °C and 900 °C resulted in a decrease in the CO_2 uptake from 7.14 to 3.56 mmol(CO_2) g(sorbent)$^{-1}$ (10 cycles), respectively. Thus, under practically relevant operation conditions the CO_2 uptake of the best material developed here, i.e., Ca_pentanol_90:10, exceeded the CO_2 uptake of the reference limestone by 200%.

3. Conclusion

We have developed CaO-based, MgO-supported CO_2 sorbents via a re-crystallization technique. We could demonstrate that re-crystallization in alcohols such as pentanol or ethanol resulted in the formation of micrometre-sized rods of calcium acetate, whereas coarse and rather heterogeneous structures were obtained for re-crystallization in alkanes or toluene. Unsupported CaO, independent of its initial morphology, showed a relatively rapid decrease in its cyclic CO_2 capture capacity, in particular under practically relevant reaction conditions. Thus, to improve the thermal stability of the morphology of the CO_2 sorbents and, in turn, its cyclic CO_2 uptake capacity, CaO was stabilized by an inert, high Tammann temperature support,

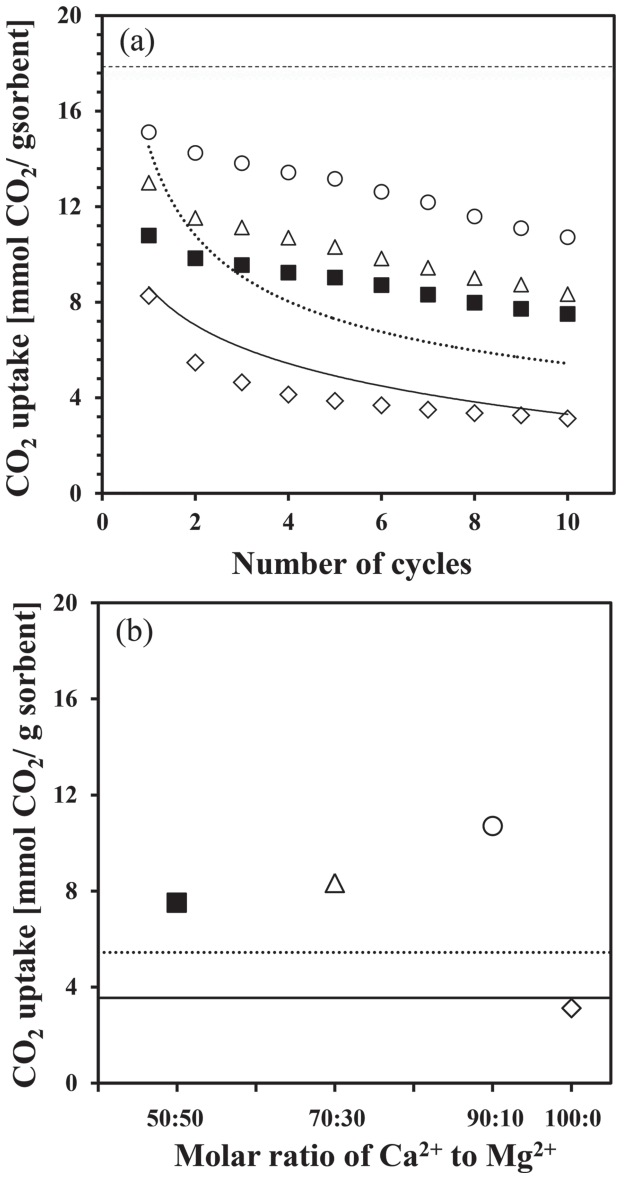

Figure 7. CO_2 uptake of the newly developed CO_2 sorbents containing different molar ratios of Ca^{2+} to Mg^{2+}: (◊) Ca_pentanol_100:0, (○) Ca_pentanol_90:10, (Δ) Ca_pentanol_70:30, (■) Ca_pentanol_50:50, (···) Ca_90:10 and (—) limestone; carbonation was performed at 650 °C (20 vol.% CO_2 in N_2) whereas calcination was performed at 900 °C using an atmosphere of 100 vol.% CO_2. The dashed line gives the theoretical CO_2 uptake of pure CaO.

viz. MgO. To achieve very favourable CO_2 uptake characteristics, even under very harsh, i.e., realistic, calcination conditions, it was found critical to mix Ca^{2+} and Mg^{2+} on a nanometer level. In addition, the current synthesis technique allows the amount of MgO required to stabilize the cyclic CO_2 uptake to be reduced to only 8 wt%. The materials developed here markedly exceeded the performance of the three reference materials, viz. limestone, commercial calcium acetate and mechanically mixed calcium and magnesium acetate. Decreasing the molar ratio of Ca^{2+} to Mg^{2+} resulted in materials with a higher surface area and pore volume, as well as an improved thermal stability of the material's morphology. However, the reduced quantity of active CaO limited the CO_2 uptake of these materials.

4. Experimental Section

4.1. Preparation of the Materials

The synthesis technique reported here was inspired by the work of Bian et al.,[34] however, critically extended to allow the "one-pot" re-crystallization of bi-component materials, i.e., containing CO_2 capture active CaO and the high Tammann temperature support MgO. In a typical synthesis, 0.01 mol of calcium acetate hydrate (in some cases together with magnesium acetate hydrate) was added to 200 mL of the solvent (alcohols, alkanes or toluene). The mixture was subsequently heated to the boiling point of the solvent and kept at this temperature for 1 h under total reflux conditions. The resulting material was washed with acetone, filtered and dried overnight at 80 °C. **Table 2** summarizes the parameter range studied here. To characterize the preparation process the following nomenclature is used: 'Ca', the abbreviation for calcium acetate, is followed by the solvent used for re-crystallization. The last number specifies the molar ratio of Ca^{2+} to Mg^{2+}.

For comparison, calcium and magnesium acetates were mechanically mixed with a molar ratio of Ca^{2+} : Mg^{2+} = 90:10 (denoted as Ca_90:10).

4.2. Characterization

4.2.1. CO_2 Capture Test

The cyclic carbonation and calcination reactions were studied using a thermogravimetric analyzer (TGA, Mettler Toledo TGA/ DSC 1). A small amount (<25 mg) of sorbent was placed in an alumina crucible and heated up to 750 °C with a rate of 10 °C $(min)^{-1}$ under a N_2 flow of 20 mL $(min)^{-1}$. Additionally, a constant N_2 flow of 25 mL $(min)^{-1}$ was used as purge flow over the micro-balance. After reaching the reaction temperature, calcination was performed for 10 min. Subsequently, a CO_2 flow of 30 mL $(min)^{-1}$ was added to the N_2 flow to carbonate the sample for 20 min. The CO_2 flow was then stopped for 20 min to re-calcine the material. For each CO_2 sorbent the carbonation and calcination cycle was repeated 10 times. The cyclic CO_2 uptake, expressed in mmol(CO_2) g$(sorbent)^{-1}$ was calculated from the continuously monitored weight change.

To investigate the influence of the calcination temperature on the CO_2 capture characteristics, the following TGA protocol was used. A small amount (<25 mg) of sorbent was placed in an alumina crucible and heated to 900 °C at a rate of 50 °C $(min)^{-1}$ under a CO_2 flow of 30 mL $(min)^{-1}$. After reaching the reaction temperature, calcination was

Table 2. Summary of the materials synthesized.

Calcium precursor	Solvent	Molar ratio Ca^{2+}:Mg^{2+}	Reflux temperature [°C]
Ca_methanol_100:0	methanol	100:0	65
Ca_ethanol_100:0	ethanol	100:0	78
Ca_pentanol_100:0	1-pentanol	100:0	137
Ca_pentane_100:0	pentane	100:0	36
Ca_hexane_100:0	hexane	100:0	69
Ca_toluene_100:0	toluene	100:0	110
Ca_pentanol_90:10	1-pentanol	90:10	137
Ca_pentanol_70:30	1-pentanol	70:30	137
Ca_pentanol_50:50	1-pentanol	50:50	137
Ca_90:10	–	90:10	–

performed for 10 min. Subsequently, the temperature was reduced to 650 °C. The carbonation reaction was performed for 20 min at 650 °C using an atmosphere containing 20 vol% CO_2. After carbonation a new cycle was started by increasing the reaction temperature to 900 °C and switching to a reactive flow of 30 mL $(min)^{-1}$ of CO_2. The carbonation and calcination cycle was repeated 10 times.

4.2.2. Structural Tests

The surface morphology of the sorbent was characterized using scanning electron microscopy (FEI Quanta 200 FEG and Zeiss Gemini 1530 FEG). A double-sided carbon tape was used to attach the sorbent onto a 12.5×10 mm aluminium holder. The sample was sputter coated (MED 010) with an approximately 8 nm-thick layer of platinum.

A Quantachrome (NOVA 4000e) analyzer was used to determine the surface area and pore volume of the material. Fresh samples were degassed at 80 °C (calcined limestone at 300 °C) for at least 3 h prior to characterization. The Brunauer et al.[35] (BET) and the Barrett et al.[36] (BJH) models, were used to calculate the surface area and pore size distribution, respectively.

Temperature programmed decomposition (TPD) experiments were performed in a thermogravimetric analyzer (TGA, Mettler Toledo TGA/ DSC 1). In a typical TPD experiment a small amount of material (<25 mg) was placed in an alumina crucible and heated up to 1000 °C at a rate of 10 °C $(min)^{-1}$ under a flow of 50 mL $(min)^{-1}$ of N_2.

The crystallinity and composition of the CaO-based CO_2 sorbents were determined using powder X-ray diffraction (Bruker, AXS D8 Advance). The X-ray diffractometer was equipped with a Lynxeye superspeed detector and operated at 40 mA and 40 kV. Each sample was scanned within the 2θ range of 10–90°. The step size was 0.025° with a time duration per step of 0.8 s.

Supporting Information

Supporting Information is available from the Wiley Online Library or from the author.

Acknowledgments

We are grateful to the Swiss National Science Foundation (Project: 200021_135457/1) and the Swiss Federal Office of Energy (Project SI/500881-01) for financial support. We also thank Mrs. Lydia Zehnder for help with the XRD measurements and the Scientific Center for Optical and Electron Microscopy (ScopeM) of ETH Zurich for providing training and access to electron microscopes.

Received: March 17, 2014
Revised: June 3, 2014
Published online: July 14, 2014

[1] International Energy Agency, *CO_2 emission from fuel combustion. Highlights*(2012 Editions)Paris, France **2012**.
[2] B. Metz, O. Davidson, H. de Coninck, M. Loos, L. Meyer, *IPCC Special Report on Carbon Dioxide Capture and Storage* Cambridge University Press, New York, USA **2005**.
[3] M. E. Boot-Handford, J. C. Abanades, E. J. Anthony, M. J. Blunt, S. Brandani, N. Mac Dowell, J. R. Fernandez, M.-C. Ferrari, R. Gross, J. P. Hallett, R. S. Haszeldine, P. Heptonstall, A. Lyngfelt, Z. Makuch, E. Mangano, R. T. J. Porter, M. Pourkashanian, G. T. Rochelle, N. Shah, J. G. Yao, P. S. Fennell, *Energy Environ. Sci.* **2014**, *7*, 130.
[4] A. M. Kierzkowska, R. Pacciani, C. R. Müller, *ChemSusChem* **2013**, *6*, 1130.
[5] M. J. Tuinier, H. P. Hamers, M. van Sint Annaland, *Int. J. Greenhouse Gas Control* **2011**, *5*, 1559.
[6] H. He, M. Zhong, D. Konkolewicz, K. Yacatto, T. Rappold, G. Sugar, N. E. David, J. Gelb, N. Kotwal, A. Merkle, K. Matyjaszewski, *Adv. Funct. Mater.* **2013**, *23*, 4720.
[7] J. Wei, D. Zhou, Z. Sun, Y. Deng, Y. Zhao, *Adv. Funct. Mater.* **2013**, *23*, 2322.
[8] M. B. Yue, Y. Chun, Y. Cao, X. Dong, J. H. Zhu, *Adv. Funct. Mater.* **2006**, *16*, 1717.
[9] M. D. Judd, M. I. Pope, *J. Appl. Chem.* **1970**, *20*, 384.
[10] J. C. Abanades, E. J. Anthony, D. Y. Lu, C. Salvador, D. Alvarez, *AIChE J.* **2004**, *50*, 1614.
[11] D. Alvarez, J. C. Abanades, *Ind. Eng. Chem. Res.* **2005**, *44*, 5608.
[12] Z. Li, H. Sun, N. Cai, *Energy Fuels* **2012**, *26*, 4607.
[13] Z. C. Sun, S. W. Luo, P. P. Qi, L. S. Fan, *Chem. Eng. Sci.* **2012**, *81*, 164.
[14] D. C. Ozcan, B. H. Shanks, T. D. Wheelock, *Ind. Eng. Chem. Res.* **2011**, *50*, 6933.
[15] N. Phalak, N. Deshpande, L. S. Fan, *Energy Fuels* **2012**, *26*, 3903.
[16] V. Manovic, D. Lu, E. J. Anthony, *Fuel* **2008**, *87*, 3344.
[17] Z. S. Li, N. S. Cai, Y. Y. Huang, H. J. Han, *Energy Fuels* **2005**, *19*, 1447.
[18] H. Lu, A. Khan, S. E. Pratsinis, P. G. Smirniotis, *Energy Fuels* **2009**, *23*, 1093.
[19] M. Broda, A. M. Kierzkowska, C. R. Müller, *ChemSusChem* **2012**, *5*, 411.
[20] R. Filitz, A. M. Kierzkowska, M. Broda, C. R. Müller, *Environ. Sci. Technol.* **2012**, *46*, 559.
[21] M. Broda, A. M. Kierzkowska, C. R. Müller, *Environ. Sci. Technol.* **2012**, *46*, 10849.
[22] M. Broda, C. R. Müller, *Adv. Mater.* **2012**, *24*, 3059.
[23] M. Broda, C. R. Müller, *Fuel* **2014**, *127*, 94–100.
[24] C. Reichardt, *Solvents and solvent effects in organic chemistry* Wiley-VCH, Weinheim, Germany **2003**.
[25] M. Durand, V. Molinier, W. Kunz, J.-M. Aubry, *Chem. Eur. J.* **2011**, *17*, 5155.
[26] A. Seidell, *Solubilities of Inorganic and Metal Organic Compounds* Van Nostrand, New York, USA **1940**.
[27] P. van der Sluis, A. Schouten, A. L. Spek, *Acta Cryst.* **1987**, *C43*, 1922.
[28] C. Saury, R. Boistelle, F. Dalemat, J. Bruggemant, *J. Chem. Eng. Data* **1993**, *38*, 56.
[29] J. C. Abanades, D. Alvarez, *Energy Fuels* **2003**, *17*, 308–315.
[30] R. H. Borgwardt, *Chem. Eng. Sci.* **1989**, *44*, 53–60.
[31] H. T. S. Britton, S. J. Gregg, G. W. Winsor, *Trans. Faraday Soc.* **1952**, *48*, 70.
[32] M. A. Carreon, V. V. Guliants, *Eur. J. Inorg. Chem.* **2005**, 27.
[33] F. N. Ridha, V. Manovic, A. Macchi, E. J. Anthony, *Int. J. Greenhouse Gas Control* **2012**, *6*, 164.
[34] S. W. Bian, J. Baltrusaitis, P. Galhotra, V. H. Grassian, *J. Mater. Chem.* **2010**, *20*, 8705.
[35] S. Brunauer, P. H. Emmett, E. Teller, *J. Am. Chem. Soc.* **1938**, *60*, 309.
[36] E. P. Barrett, L. G. Joyner, P. P. Halenda, *J. Am. Chem. Soc.* **1951**, *73*, 373.